

# Fabrication of $\text{Si}_{1-x}\text{Ge}_x$ Alloy on Silicon by Ge-Ion-Implantation and Short-Time-Annealing

K. GAO\*, S. PRUCNAL, A. MÜCKLICH, W. SKORUPA AND S. ZHOU

Institute of Ion Beam Physics and Materials Research, Helmholtz-Zentrum Dresden-Rossendorf (HZDR)

P.O. Box 510119, 01314 Dresden, Germany

In our contribution we present the fabrication of  $\text{Si}_{1-x}\text{Ge}_x$  alloy by ion-implantation and millisecond flash lamp annealing. The 100 keV Ge ions at the fluence of  $10 \times 10^{16}$ ,  $5 \times 10^{16}$ , and  $3 \times 10^{16} \text{ cm}^{-2}$  were implanted into monocrystalline (100)-oriented Si wafers covered by 50 nm thermal oxide. In the consequence, the 50 nm amorphous Ge rich Si layers were obtained. The recrystallization of the implanted layers and the  $\text{Si}_{1-x}\text{Ge}_x$  alloying were accomplished by flash lamp annealing with the pulse duration of 20 ms. Flash lamp treatment at high energy densities leads to local melting of the Ge-rich silicon layer. Then the recrystallization takes place due to the millisecond range liquid phase epitaxy. Formation of the high quality monocrystalline  $\text{Si}_{1-x}\text{Ge}_x$  layer was confirmed by the  $\mu$ -Raman spectroscopy, the Rutherford backscattering channeling and cross-sectional transmission electron microscopy investigation. The  $\mu$ -Raman spectra reveal three phonon modes located at around 293, 404, and  $432 \text{ cm}^{-1}$  corresponding to the Ge-Ge, Si-Ge and Si-Si in the  $\text{Si}_{1-x}\text{Ge}_x$  alloy vibrational modes, respectively. Due to much higher carrier mobility in the  $\text{Si}_{1-x}\text{Ge}_x$  layers than in silicon such system can be used for the fabrication of advanced microelectronic devices.

DOI: [10.12693/APhysPolA.123.858](https://doi.org/10.12693/APhysPolA.123.858)

PACS: 61.72.uf, 78.55.Ap, 68.37.Lp

## 1. Introduction

Silicon-germanium ( $\text{Si}_{1-x}\text{Ge}_x$ ) alloying can tailor the electronic properties of silicon to improve the performance of microelectronic devices (e.g., heterojunction bipolar transistors and CMOS transistors). Up to now mainly epitaxial methods (e.g., chemical vapor deposition, molecular beam epitaxy) are applied in the synthesis of  $\text{Si}_{1-x}\text{Ge}_x$  alloys [1, 2]. Ge-ion-implantation into the Si wafer followed by subsequent annealing is an efficient commercial method to synthesize  $\text{Si}_{1-x}\text{Ge}_x$  [3–7]. In this paper we propose the realization of a compact, CMOS compatible and fully integrated solution for the integration of the SiGe alloys in silicon technology for electronic applications. The  $\text{Si}_{1-x}\text{Ge}_x$  layer is synthesized in silicon wafers using the combined ion beam implantation and millisecond flash lamp annealing (FLA) techniques. The energy budget introduced to the sample during FLA is sufficient to recrystallize the amorphized layer due to ion-implantation and to form  $\text{Si}_{1-x}\text{Ge}_x$  alloy. Successful formation of the  $\text{Si}_{1-x}\text{Ge}_x$  layer was confirmed by  $\mu$ -Raman spectroscopy and cross-sectional transmission electron microscopy (TEM). Moreover, the data obtained by the Rutherford backscattering spectrometry (RBS) in random and channeling conditions shows the formation of quasi-epitaxial  $\text{Si}_{1-x}\text{Ge}_x$  layer on Si.

## 2. Experimental setup

Single-crystalline *n*-type (100) silicon wafers covered with 50 nm of a dry-grown thermal oxide layer were im-

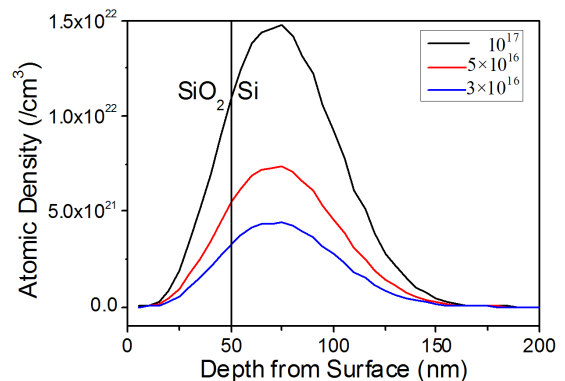


Fig. 1. Atomic densities of Ge as the functions of depth from the surface of the Si wafer after implantation with the kinetic energy of 100 keV and the fluence of  $3 \times 10^{16}$ ,  $5 \times 10^{16}$ ,  $10 \times 10^{16} \text{ cm}^{-2}$ . The results were simulated by the SRIM code [8].

planted with the Ge ions at the energy of 100 keV and the fluence of  $1 \times 10^{17}$ ,  $5 \times 10^{16}$ ,  $3 \times 10^{16} \text{ cm}^{-2}$  (the corresponding samples will be referred to as 1E17, 5E16, and 3E16, respectively). In a consequence, the amorphous Ge-rich Si layers were obtained. Figure 1 shows the predicted depth profile of Ge atoms in the  $\text{SiO}_2/\text{Si}$  system in the as-implanted stage. From the peak concentration of the samples, the  $x$  values for  $\text{Si}_{1-x}\text{Ge}_x$  are calculated to be 0.23, 0.13, and 0.081, respectively. The recrystallization of the implanted layers and the  $\text{Si}_{1-x}\text{Ge}_x$  alloying were carried out by flash lamp annealing for 20 ms. In such stage flash lamp treatment at high energy densities heats the surface above  $1400^\circ\text{C}$  hence leading to local melting of the Ge-rich silicon layer within several hun-

\*corresponding author; e-mail: [k.gao@hzdr.de](mailto:k.gao@hzdr.de)

dreds nanometers' range, whereas the rest of the wafer remains cold. Then due to such significant temperature differences, the molten layer starts to cool down in the millisecond range, which results in the bottom-up liquid phase epitaxial growth of the  $\text{Si}_{1-x}\text{Ge}_x$  layer.

The optical and structural properties of the  $\text{Si}_{1-x}\text{Ge}_x$  alloy were investigated by means of  $\mu$ -Raman spectroscopy. The  $\mu$ -Raman spectra were performed in a backscattering geometry with a 532 nm Nd:YAG laser excitation, and detected by a liquid- $\text{N}_2$ -cooled charge-coupled device. The Ge distribution and crystallinity of the  $\text{Si}_{1-x}\text{Ge}_x$  layer after implantation and annealing were evaluated by the RBS. The RBS spectra were collected with a collimated 1.7 MeV  $\text{He}^+$  beam at a backscattering angle of  $170^\circ$ . The sample was mounted on a three-axis goniometer with the precision of  $0.01^\circ$ . The channeling spectra were collected by aligning the sample to make the impinging  $\text{He}^+$  beam parallel with the  $\text{Si}\langle 001 \rangle$  axis. Moreover, the microstructural properties of the  $\text{Si}_{1-x}\text{Ge}_x$  alloy were investigated by the cross-sectional TEM. The TEM images were taken by means of an FEI Titan 80-300 scanning transmission electron microscope operating at 300 keV.

### 3. Results and discussion

#### 3.1. Raman spectra

The optical properties of the  $\text{Ge}^+$ -implanted and flash lamp annealed samples were investigated by means of  $\mu$ -Raman spectroscopy. Figure 2 shows the  $\mu$ -Raman spectra obtained from the implanted and FLA annealed samples at  $1400^\circ\text{C}$  for 20 ms. According to the absorption coefficient  $\alpha$  for  $\text{Si}_{1-x}\text{Ge}_x$  ( $x = 0.228, 0.129, 0.081$ ), reported by Humlicek et al. [9], the penetration depth for 532 nm (2.41 eV) light is estimated to be more than 100 nm. Therefore, the Raman spectra exhibit the information about the  $\text{Si}_{1-x}\text{Ge}_x$  alloy layer and the silicon substrate with the main peak located at  $520.5\text{ cm}^{-1}$  attributed to the scattering of Si longitudinal optical (LO) phonon mode.

Besides the LO phonon mode, the silicon substrate shows the peak at  $303\text{ cm}^{-1}$  originating from the second-order transverse acoustic phonon (2TA) scattering mode. In the case of the sample implanted at  $10 \times 10^{16}\text{ cm}^{-2}$ , after annealing the Raman spectra show three peaks at about  $286\text{ cm}^{-1}$ ,  $403\text{ cm}^{-1}$ , and  $508\text{ cm}^{-1}$  corresponding to the first-order Raman scattering from the  $\text{Si}_{1-x}\text{Ge}_x$  layer: Ge-Ge, Si-Ge, and Si-Si atomic vibration bonds, respectively [10, 11]. In addition, there is another peak at around  $430\text{ cm}^{-1}$ , which is related to the local Si-Si phonon mode due to compositional disorder and localization in the  $\text{Si}_{1-x}\text{Ge}_x$  layer [9, 12, 13].

For the samples 3E16 only a weak phonon mode at around  $430\text{ cm}^{-1}$  due to the Si-Si atomic vibration bonds in the SiGe layer was observed. The Si-Ge related atomic vibration bonds were seen from the samples implanted with the fluence of  $5 \times 10^{16}\text{ cm}^{-2}$  which is the minimum

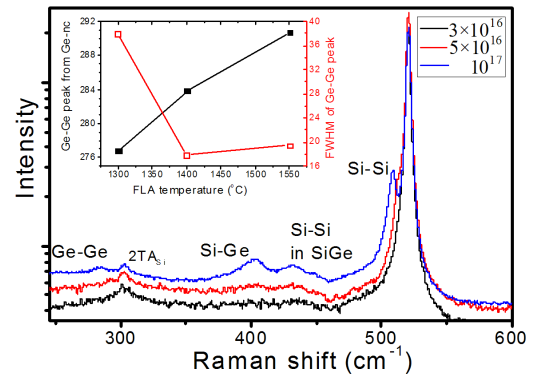


Fig. 2.  $\mu$ -Raman spectra obtained from the flash lamp annealed samples for 20 ms at  $1400^\circ\text{C}$ . Several characteristic peaks of  $\text{Si}_{1-x}\text{Ge}_x$  are clearly depicted. The inset shows the change of the Ge-Ge related phonon mode position and FWHM as the function of annealing temperature.

fluence needed for efficient  $\text{Si}_{1-x}\text{Ge}_x$  alloy layer formation.

The inset in Fig. 2 shows the change of the Ge-Ge related phonon mode position as the function of annealing temperature. This Ge-Ge mode was clearly seen only from the samples 1E17 annealed at a temperature higher than  $1200^\circ\text{C}$ . With increasing annealing temperature from 1300 up to  $1550^\circ\text{C}$ , the position of the Ge-Ge related phonon mode shifts from  $277$  to  $291\text{ cm}^{-1}$  and the FWHM decreases from  $38$  to  $18\text{ cm}^{-1}$ . That vibration phonon mode was ascribed to the Ge nanocrystals formed in the oxide layer close to the  $\text{SiO}_2/\text{Si}$  interface. The bulk crystalline Ge has a phonon mode at  $300.7\text{ cm}^{-1}$  [14]. But due to the quantum confinement effect, the peak position of this phonon mode in the Ge nanocrystals shifts to the lower frequency. Hence we can conclude that the observed Ge-Ge related phonon mode is due to the Ge nanocrystals whose sizes increase with the increasing annealing temperature. In the meanwhile, a decrease of the FWHM shows an improvement of the nanocrystals quality by the strain reduction within the Ge nanocrystals.

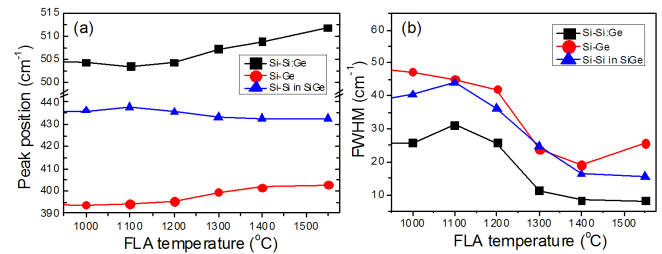


Fig. 3. The shift of the main phonon mode peak position in the  $\text{Si}_{1-x}\text{Ge}_x$  alloy as the function of annealing temperature (a) and FWHM of the related peaks (b) obtained from the sample implanted with the fluence of  $1 \times 10^{17}\text{ Ge}^+/\text{cm}^2$ .

Figure 3a shows the peak position evolution of the main phonon modes in the  $\text{Si}_{1-x}\text{Ge}_x$  alloy as functions of annealing conditions. In the case of the Si–Ge phonon mode, the peak shifts from  $393.8$  to  $402.9\text{ cm}^{-1}$  which is an evidence for better alloying and for the increase of Ge concentration in the  $\text{Si}_{1-x}\text{Ge}_x$  layer. The Si–Si:Ge (Si–Si bonds surrounded by the Ge atoms) phonon mode shows the same behavior. The position shift of the Si–Si vibration phonon mode in SiGe to the lower frequency (from  $436$  to  $432\text{ cm}^{-1}$ ) indicates improvement of the  $\text{Si}_{1-x}\text{Ge}_x$  layer and such behavior is typical of the samples with higher Ge concentration. Improvement of the crystal quality with the increasing annealing temperature is also confirmed by the decrease of the FWHM of the main Si–Ge related phonon modes (see Fig. 3b). From these discussed features,  $1400\text{ }^\circ\text{C}$  is determined to be the best annealing temperature.

### 3.2. Rutherford backscattering spectra

Figure 4 shows the RBS random and the channeling spectra along the  $\langle 001 \rangle$  direction for the FLA  $\text{Si}_{1-x}\text{Ge}_x$  samples at  $1400\text{ }^\circ\text{C}$ . Before test the  $\text{SiO}_2$  layers were removed by chemical etching. From the random spectra the Ge penetration depth is calculated. For both samples, the Ge concentration is roughly uniform from the surface to around  $50\text{ nm}$  depth. At the higher energy side (i.e. the sample surface) the Ge distribution shows a sharper edge. This is because the  $\text{SiO}_2$  layers on top were removed so that the higher Ge concentration layer was directly exposed on top of the wafer. In the deeper region, the Ge concentration remains the Gaussian shape, which is consistent with the SRIM results discussed above. From the channeling spectra (Si signal), near the surface there are two peaks. The one at higher energy is the signal of Si in the  $\text{Si}_{1-x}\text{Ge}_x$  layer, as a consequence of the disorder in the alloy; whereas the deeper one is from the interface

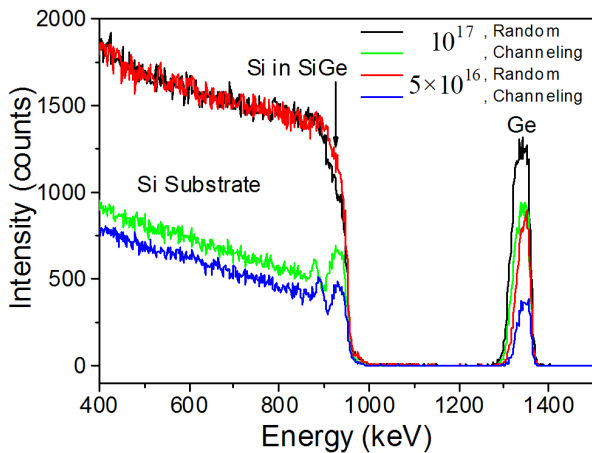


Fig. 4. RBS random and channeling spectra of FLA  $\text{Si}_{1-x}\text{Ge}_x$  for Ge implantation fluence of  $10 \times 10^{16}$  and  $5 \times 10^{16}\text{ cm}^{-2}$ . The channeling effect clearly suggests the recrystallization of the amorphous  $\text{Si}_{1-x}\text{Ge}_x$  layer after FLA.

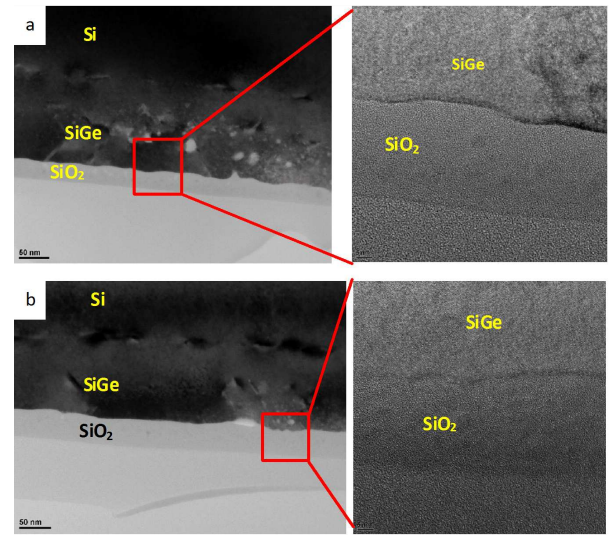


Fig. 5. (a), (b) Cross-sectional transmission electron microscopy images of the sample 1E17 (a) and 5E16  $\text{cm}^{-2}$  (b).  $\text{SiO}_2$  and  $\text{Si}_{1-x}\text{Ge}_x$  layers show distinct differences.

between the molten layer and the region remained solid phase during FLA. For the sample 5E16, the Ge depth is slightly shallower and the Ge-implanted thickness is thinner than the  $10 \times 10^{16}\text{ cm}^{-2}$  implanted one, which shows differences from the theoretical results calculated by SRIM discussed above.

### 3.3. Cross-sectional transmission electron microscopy

Cross-sectional transmission electron microscopy was used to examine the crystallinity and depth profile of the  $\text{Si}_{1-x}\text{Ge}_x$  alloys (see Fig. 5). Beneath the surface the  $\text{Si}_{1-x}\text{Ge}_x$  layer with good planarity is clearly shown for both samples. In the magnified images typical crystallized structures are depicted, which is consistent with the RBS channeling spectra. Moreover, the high temperature annealed samples show the Ge nanocrystals formation in the  $\text{SiO}_2$  layer which is consistent with the data obtained by the  $\mu$ -Raman spectroscopy.

## 4. Conclusions

In this contribution, we have successfully synthesized the  $\text{Si}_{1-x}\text{Ge}_x$  alloys with different Ge concentrations by the two efficient commercial methods: Ge-ion-implantation and millisecond flash lamp annealing. The Raman spectra suggest the formation of bonds between Si–Si, Si–Ge, and Ge–Ge; whereas the RBS channeling spectra as well as the cross-sectional TEM images give further evidence for the crystallized  $\text{Si}_{1-x}\text{Ge}_x$  alloys after annealing.

### Acknowledgments

This work was supported by the Helmholtz–Gemeinschaft Deutscher Forschungszentren (HGF-VH-NG-713).

## References

- [1] S.-M. Jang, K. Liao, R. Reif, *J. Electrochem. Soc.* **142**, 3520 (1995).
- [2] G.L. Patton, S.S. Iyer, S.L. Delage, S. Tiwari, J.M.C. Stork, *IEEE Electron. Dev. Lett.* **9**, 165 (1988).
- [3] F. Corni, S. Frabboni, G. Ottaviani, G. Queirolo, D. Bisero, C. Bresolin, R. Fabbri, M. Servidori, *J. Appl. Phys.* **71**, 2644 (1992).
- [4] X. Lu, N.W. Cheung, *Appl. Phys. Lett.* **69**, 1915 (1996).
- [5] M. Voelskow, R. Yankov, W. Skorupa, J. Pezoldt, T. Kups, *Appl. Phys. Lett.* **93**, 151903 (2008).
- [6] M. Voelskow, A. Kanjilal, W. Skorupa, *Curr. Appl. Phys.* **10**, 1309 (2010).
- [7] M. Voelskow, I. Stoimenos, L. Rebohle, W. Skorupa, *Phys. Status Solidi C* **8**, 960 (2011).
- [8] J.F. Ziegler, *Nucl. Instrum. Methods Phys. Res. B* **219-220**, 1027 (2004).
- [9] J. Humlíček, M. Garriga, M.I. Alonso, M. Cardona, *J. Appl. Phys.* **65**, 2827 (1989).
- [10] A. Picco, E. Bonera, E. Grilli, M. Guzzi, M. Giarola, G. Mariotto, D. Chrastina, G. Isella, *Phys. Rev. B* **82**, 115317 (2010).
- [11] T.S. Perova, J. Wasyluk, K. Lyutovich, E. Kasper, M. Oehme, K. Rode, A. Waldron, *J. Appl. Phys.* **109**, 033502 (2011).
- [12] E. Bonera, F. Pezzoli, A. Picco, G. Vastola, M. Stoffel, E. Grilli, M. Guzzi, A. Rastelli, O.G. Schmidt, L. Miglio, *Phys. Rev. B* **79**, 075321 (2009).
- [13] G. Isella, D. Chrastina, B. Rössner, T. Hackbarth, H.J. Herzog, U. König, H. von Känel, *Solid-State Electron.* **48**, 1317 (2004).
- [14] J.H. Parker, Jr., D.W. Feldman, M. Ashkin, *Phys. Rev.* **155**, 712 (1967).